Proceedings of the 21st ICSMGE, Vienna, Austria, 14 – 19 June 2026. Pistrol, Adam & Schweiger (eds.)
Published by: ÖGG, Austrian Society for Geomechanics, Salzburg, Austria, ISBN 978-3-9503898-4-5
https://doi.org/10.53243/ICSMGE2026-2352

Preliminary investigation on the vertical tip bearing capacity mechanism of steel pipe sheet-pile foundations

Kei Katayama
CHODAI CO.,LTD, Japan, Tsukuba, kataya-k@chodai.co.jp

Takashi Matsushima
Tsukuba University, Japan

ABSTRACT: This study aims to clarify the tip bearing capacity characteristics of steel pipe sheet-pile foundations by conducting virtual loading test simulations using the two-dimensional discrete element method (2D DEM). Open-ended and closed-ended single piles and three-pile arrangements were used as models. The soil particle models were correlated with standard penetration test (SPT) N-values, and analytical simulations were carried out. Results showed that in both single and three-pile models, over 80% of the tip bearing capacity was borne by the pipe tip compared to the internal soil. Additionally, the group-pile reduction ratio was 81% for open-end piles and 67% for closed-end piles, indicating that group-pile effects are more significant in the latter. This paper presents an initial investigation; sensitivity analyses on joint-pipe effects, soil–N-value correlations, and particle-scale phenomena will be reported based on forthcoming 3D DEM simulations and physical model tests ahead of the presentation.

KEYWORDS: steel pipe sheet-pile foundation; tip bearing capacity; discrete element method; group-pile effect.

1 INTRODUCTION

Steel pipe sheet-pile foundations consist of steel pipe piles connected by joint pipes and driven continuously into the ground in a caisson-like configuration. This foundation type, originally developed in Japan, is widely used in overseas assistance projects. However, the bearing capacity of such foundations has traditionally been verified based on single open-ended piles, and further studies have not been conducted. In this study, virtual loading tests using a 2D DEM simulation were performed with a three-pile arrangement representing a simplified model of a steel pipe sheet-pile foundation. By comparing to single open-ended piles, the tip bearing capacity mechanism the mechanism is visualized and analyzed at the particle level, with a focus on the influence of contact forces and particle movements around the pile tip.

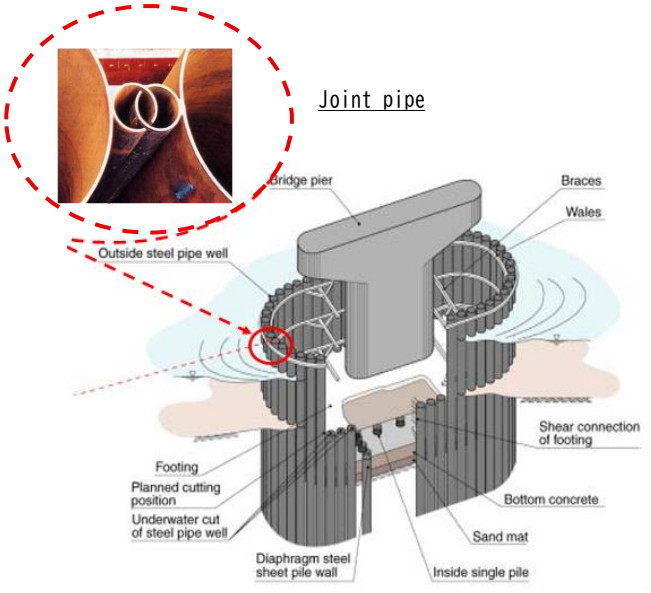

Figure 1. Conceptual diagram for steel pipe sheet-pile foundation

2 OVERVIEW OF DEM ANALYSIS MODEL

2.1 *Analysis Approach Previous*

FEM analyses indicated that over 80% of the tip bearing capacity was carried by the pipe tip compared to the internal soil. In addition, group-pile simulations using closed-ended piles showed a significant group effect, with each pile bearing only about half the capacity of a single pile. Building on these findings, DEM analysis was used to investigate the tip bearing mechanism by comparing single piles and three-pile arrangements that include joint pipes, simulating part of the sheet-pile foundation.

2.2 *Analysis Model*

To match existing bearing capacity formulas that relate to N-values, a two-layer ground model is considered (Figure 3). The first layer is a 5.0 m thick sand layer with N = 10 and unit weight γ = 17 kN/m³. For modeling purposes, the unit weight is quadrupled to 68 kN/m³ to represent 20 m of overburden. The second layer is a 15.0 m thick bearing layer with N = 50, unit weight γ = 19 kN/m³, and internal friction angle φ = 30°.

2.3 *Soil Particle Model*

Instead of using circular particles without rotational resistance, particles are modeled by combining two circular elements. A dynamic optimization algorithm is used to determine the position and radius of the elements to match the 2D shapes of 50 Touura sand grains obtained via digital microscopy (Figure 2).

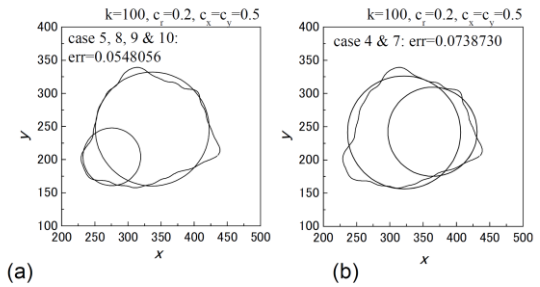

Figure 2. Model of a single particle reproduced by two circular elements.

DEM analysis was performed using a program adopted from NUMGE (2002), with 23,501 particles (47,280 circular elements) and 1,281 segment elements representing the piles and joint pipes. The model scale is 100 times the actual sand particles. The soil chamber is formed by random dropping particles of 100 to 200 mm size, bounded by fixed 250 mm diameter circular elements.

2.4 *Analysis Parameters*

Soil parameters were derived using the empirical relationship between SPT N-values and shear wave velocity (V_{SDi}) from the Road Bridge Design Specifications:

$$V_{SDi} = c_v V_{Si} \quad (1)$$

$$V_{Si} = 80N^{1/3} \quad (1 \le N \le 50) \quad (2)$$

Here, V_{si} is the average shear-wave velocity of the i-th layer, c_v is a strain-based correction factor (0.8), and N is the SPT N-value. The normal and tangential spring stiffnesses (kn, ks) between connected circular elements were calculated using Hakuno's empirical formulas:

$$k_\alpha = \frac{1}{4}\pi\rho V_\beta^2 \quad (\alpha = n, s;\ \beta = p, s) \quad (3)$$

$$V_P/V_s = \sqrt{2(1-\nu)/(1-2\nu)} \quad (4)$$

Here, α = n, s denotes normal and tangential directions, $\beta = p, s$ denotes compressional and shear waves, ρ is the density, and ν is Poisson's ratio. Poisson's ratio is set to 0.4 for the surface layer and 0.45 for the bearing layer. Next, the viscous damping coefficients in the normal and tangential directions (c: damping stiffness) were also determined using Hakuno's proposed expression as follows:

$$c_\alpha = 2h\sqrt{k_\alpha m} \quad (\alpha = n, s) \quad (5)$$

where h = 1 for critical damping, and m is the element mass. The calculated analysis parameters are listed in Table 1.

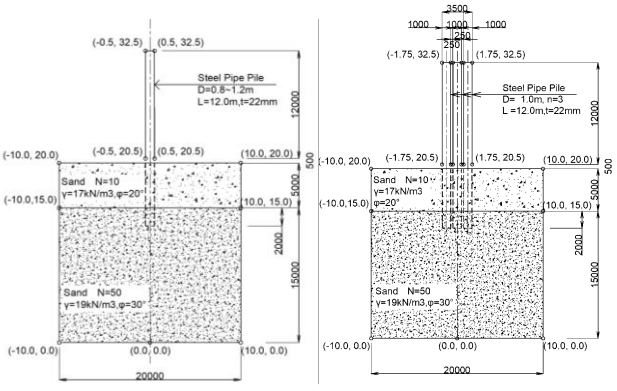

- a) Single pile
  - a-1) Open-end
- b) Three-pile arrangement
  - b-1) Open-end
  - b-2) Closed-end

Figure 3. Comparison of virtual load-test models.

Boundary conditions used fixed 200 mm diameter circular elements with bearing-layer material parameters, but with spring constants reduced by one order of magnitude and damping coefficients increased by one order to simulate boundary absorption. The piles, being much stiffer, used the same parameters as the bearing layer to avoid numerical artifacts.

The inter-particle friction angle φ was set based on the 100× scale: 20° for the surface layer (lower bound) and 23° for the bearing layer to differentiate behavior between layers.

3 INVESTIGATION OF VIRTUAL LOADING TESTS

3.1 *Analysis Conditions and Procedure*

3.1.1 *Analysis Cases and Procedure*

The analysis will be conducted on the three cases shown in Figure 3.

All piles have a diameter of 1.0 m, wall thickness of 22 mm, and length of 12.0 m. For the three-pile models, each pile is embedded two diameters (2 m) into the bearing layer and allowed to "stabilization period"—that is, the model is held static—for a duration determined by the curing time tests. After curing, to evaluate group-pile effects, all three piles are driven simultaneously by an additional 0.1 m (1% of pile diameter), and the ultimate tip bearing capacity is recorded. In the closed-end case, after installing the open-ended three-pile model, the soil particles inside the pipe tips are solidified so that the steel pipe and the trapped soil behave as a single unit during loading.

3.1.2 *Comparison of Embedding Speed*

The embedding speed in DEM simulations is governed by the time step and the number of steps. Higher speeds enhance dynamic effects and cause rapid increases in particle contact forces, while excessively low speeds increase numerical error and computation time. To identify the optimal embedding speed, the single open-ended pile model (1.0 m diameter, 2.0 m embedment into the bearing layer, total embedment 7 m) was used with a constant time step of 1.0×10^{-5} s. Simulations were performed at speeds from 350 m/s down to 0.7 m/s. Figure 4 shows that speeds of 3.5 m/s and above produce responses close to those from static analysis. Therefore, 3.5 m/s was adopted for all subsequent analyses.

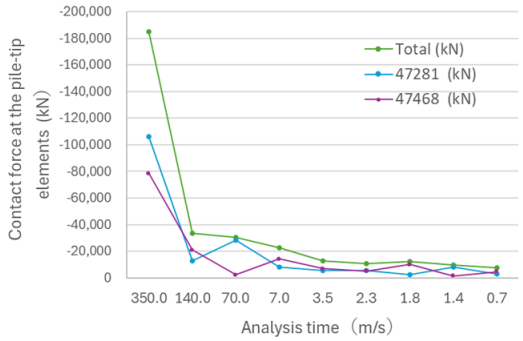

Figure 4. Comparison of Analysis Speeds During Pile Driving

Table 1. DEM Analysis Parameters

	Element Density	Element Mass	Dy. Poisson's Ratio	N-Value	Damping Constant	Shear Wave Velocity		Spring Constants		Damping Coefficients		Interparticle friction angle
	ρ	m	ν	N	h	Vp	Vs	kn	ks	c_n	c_s	φ
	kg/m^3	kg	–	–	—	m/sec	m/sec	Nm/m	Nm/m	Nsec/m	Nsec/m	deg
2nd Layer	2,640	82.9	0.40	50	0.002	578	236	6.9E+08	1.2E+08	4.8E+02	2.0E+02	23
1st Layer	8,000	251.2	0.45	10	0.002	457	138	3.3E+08	3.0E+07	3.8E+02	1.1E+02	20
Boundary	2,640	82.9	0.40	-	-	-	-	6.9E+07	1.2E+07	4.8E+03	2.0E+03	5
Pile	7,870	247.1	0.30	-	0.002	578	236	6.9E+08	1.2E+08	4.8E+02	2.0E+02	23

3.1.3 *Comparison of Curing Duration and Loading Rate*

For the single open-ended pile model, curing durations from 0.1 s to 3.0 s were tested using the two tip elements (element Nos. 47281 and 47468). Figure 5 presents the Y-direction contact force history for a 3.0 s stabilization period period: initially high contact forces dissipate through small oscillations until convergence. The rapid decay is attributed to undrained conditions (no fluid flow) and the absence of particle crushing. Since the case stabilization period for 3.0 s showed sufficient convergence, this duration was used for all models.

Loading rates were compared at 0.1 m/s and 0.3 m/s (time step 1.0×10^{-5} s, penetration increment 0.1 m). As no significant difference was observed and the 0.3 m/s curve appeared smoother, 0.3 m/s was selected as the loading speed.

3.2 *Simulation Results of Load Tests*

3.2.1 *Verification of Energy in the DEM Analysis*

In DEM, the energy balance after the analysis can be used to verify appropriateness. Figure 6 shows the relationship between the step count and various energy components: the total potential energy of the particles (engr), the kinetic energy of the particles (enva), strain energy stored in the contact springs (enka), energy dissipated by viscous damping (enca), energy dissipated by friction (enxd), and energy balance error (err). Here, the energy balance error (err) remains small at all steps, and no large oscillations or anomalies are observed, indicating a consistent and valid energy balance throughout the analysis. Additionally, almost all the work done by pile driving is dissipated by friction between the particles, while the effect of viscous damping is minimal.

3.2.2 *Simulation Results of Load Tests*

Tip Bearing Characteristics of the Open-Ended Single Pile Prior to loading, the ultimate tip bearing capacity Rt was assumed to decompose into contributions as depicted in Figure 7:

$$Rt = Rp + Rs + Rfe \tag{6}$$

where Rp is the steel-pipe wall-tip resistance, Rs is the soil resistance at the tip, and Rfe is the frictional resistance on the outer wall over one pile diameter. Furthermore,

$$Rs = Rfi + W \tag{7}$$

where Rfi is the internal friction resistance from soil adhering to the inner wall of the tip and W is the self-weight of the trapped soil.

Figure 8 shows the load–settlement curve for the single pile: elastic behavior is maintained even at a settlement equal to 10% of the pile diameter (the criterion for ultimate limit). The ratio Rp/Rt remains between 85% and 90%, gradually decreasing as settlement advances and the contribution of Rs increases.

3.2.3 *Tip Bearing Characteristics of the Sheet-Pile Foundation*

The analysis results are summarized in Table 2. In the open-ended case, the reduction ratio due to group-pile effects (group-pile effect) is 0.81 when comparing the single pile to the three-pile arrangement; in the closed-ended case, this coefficient falls to 0.68. This demonstrates that the tip bearing capacity depends strongly on whether the pile tip is open or closed.
Moreover, the reduction ratio for the closed-ended piles closely matches the trend observed in the aforementioned 3D FEM analysis[1].

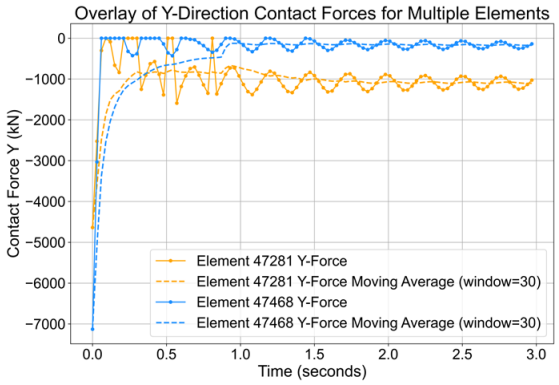

Figure 5. Time history of contact force in the Y-direction at the tip elements during the curing period(3s).

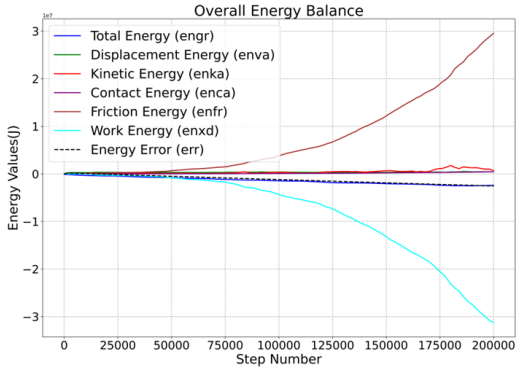

Figure 6. Energy balance during pile penetration.

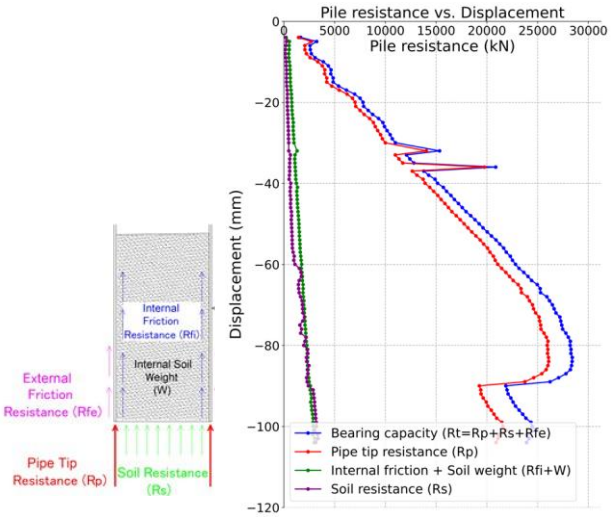

Figure 7. Decomposition of tip bearing resistance components.

Figure 8. Load–displacement curve comparison (single-pile model).

Table 2. Comparison of tip bearing capacity between single pile and triple-row pile

	Single pile	b) Three - pile（at Center pile）	
	a-1) Open-end	b-1) Open-end	b-2) Closed-end
Pile Tip Resistance Rt(kN)=①+②	28,412	23,054	19,185
	(1.00)	**(0.81)**	**(0.68)**
①Pilpe Tip Rp(kN)	25,504	21,360	15,400
	(1.00)	(0.84)	(0.60)
②Soil Redistance Rs(kN)	2,870	1,503	3,785
	(1.00)	(0.52)	(1.32)

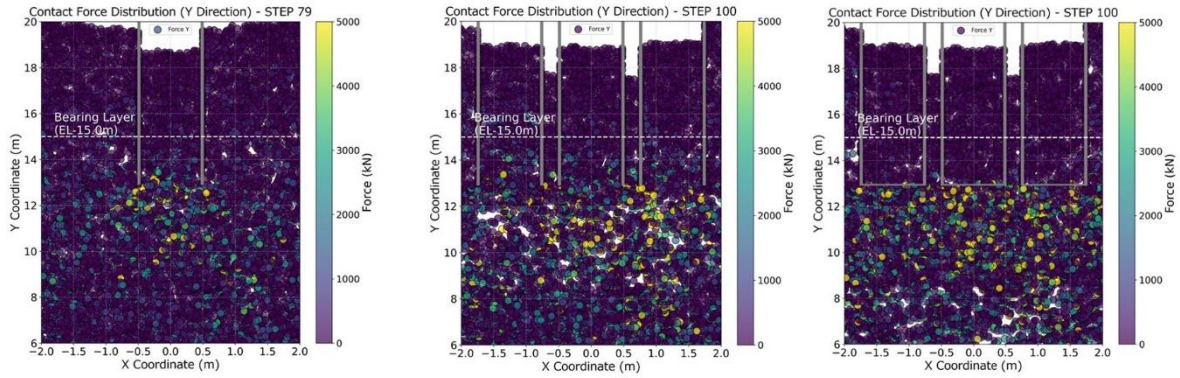

a)_Single Pile (Open-end) b)-1 Three-Pile (Open-end) b)-2 Three-Pile (Closed-end)

Figure 9. Comparison of contact force distribution around the pile tip for soil particles (at the moment of maximum Y-direction tip bearing capacity during the loading test). The circles represent the positions where contact forces occur; they are not the actual soil particles. The display area focuses on the pile tip, and the aspect ratio has been adjusted accordingly.

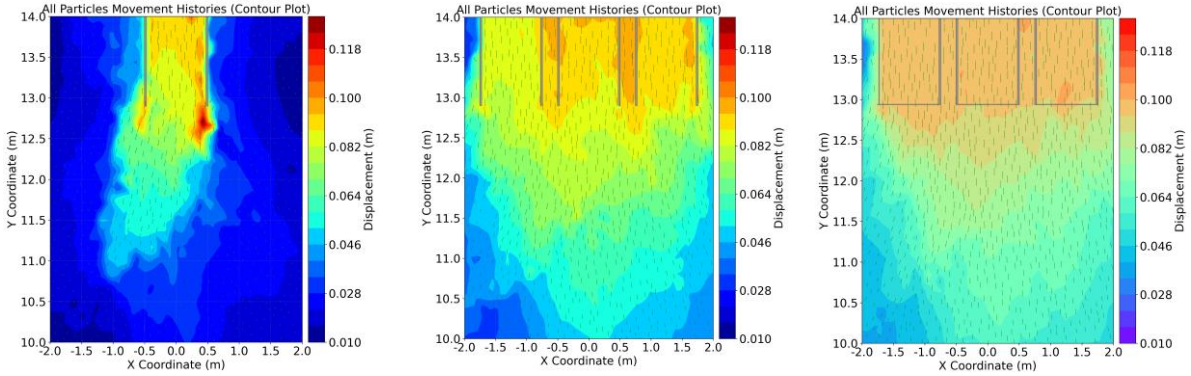

a)_Single Pile (Open-end) b)-1 Three-Pile (Open-end) b)-2 Three-Pile (Closed-end)

Figure 10. Comparison of soil particle movement history around the pile (from start to end of the loading test).
The movement history is shown as a contour map alongside particle displacements, focusing on the pile tip and with the aspect ratio adjusted accordingly.

3.2.4 *Bearing capacity characteristics of steel pipe sheet-pile foundations*

The following considerations are made based on the contact force and movement history of soil particles.

- **Comparison between open-ended and Closed-ended piles in a three-pile group:** As shown in Figures 9 b)-1 and 9 b)-2, in the open-ended model high contact forces concentrate at each individual pipe tip. In contrast, the closed-ended model exhibits a broader distribution of high contact forces across the entire bundled tip region. Likewise, in Figures 10 b)-1 and 10 b)-2, soil particle displacements remain localized around each pipe tip in the open-ended case, whereas in the closed-ended case displacements spread uniformly over the entire tip area, resembling the behavior of a single large-diameter pile.
- **Comparison between single pile and three-pile group:** For the open-ended piles, the concentration of resisting soil particles at each tip limits interference between adjacent piles, so the reduction in bearing capacity due to group-pile effects remains modest. Conversely, in the closed-ended three-pile model, particle movements overlap and interfere with resisting particles on neighboring piles, producing a pronounced group-pile effect that lowers the ultimate tip bearing capacity.

4 CONCLUSIONS

DEM-based virtual loading tests yielded these findings:

- Regions of high contact force and large displacement are strongly correlated with tip bearing capacity.
- Open-ended piles carry 80–90% of tip capacity through the pipe tip alone, regardless of internal soil conditions.
- Group-pile effects are limited for open-end sheet-pile foundations due to concentrated tip resistance.
- Closed-end configurations exhibit pronounced group-pile effects from overlapping particle movements.

Comparing past load-test averages on 1.0 m piles ($q_t \approx 7{,}000$ kN/m²) with current DEM ultimate pressures ($q_u = 27{,}131$–$36{,}194$ kN/m²) indicates a scale factor of 4.0–5.0. Given the observed scale and 2D effects, future work will refine particle scaling and perform 3D DEM simulations to validate versus SPT N-values.

5 REFERENCES

Bridge Structure Research Group, Structure Maintenance Research Center, National Institute for Land and Infrastructure Management (NILIM), 2018. Revision and evaluation of estimation methods for axial bearing capacity and spring constants of piles. NILIM Report No. 4374, pp. 28–29.

Hakuno, M., 2018. Simulation of fracture: Tracking fracture using the extended discrete element method. Morikita Publishing Co., Ltd., pp. 42–44.

Japan Road Association, 2017. Specifications for highway bridges, Part V: Seismic design. Japan Road Association, pp. 69, 89.

Katayama, K., 2024. Investigation on the vertical pile bearing characteristics of incomplete closure state of initial steel pipe piles. In: Proceedings of the 59th Annual Conference on Geotechnical Engineering. Japanese Geotechnical Society, Japan.

Matsushima, T. and Saomoto, H., 2002. Discrete element modeling for irregularly shaped sand grains. In: Mestat (ed.), Numerical Methods in Geotechnical Engineering, pp. 239–246.